Resumen

La microestructura y propiedades mecánicas de una alúmina/circona con función gradiente preparado con deposición electroforética fueron estudiadas. La microestructura fue observada por microscopia electrónica para caracterizarla con respeto a las fases, a los tamaños de granos y a su distribución. El material tenía una microestructura fina de alta cualidad con muy poca porosidad y una distribución uniforme de ZrO_2 dentro de las capas. Las propiedades mecánicas como dureza, tenacidad, pero principalmente tensiones residuales, formados como una consecuencia de las diferencias de coeficientes de expansión térmica, fueron estudiadas por métodos de indentaciones. El material exhibió una dureza excelente en las capas exteriores, comparable a la de alúmina pura. Las tensiones residuales fueron también calculadas utilizando el método de elementos finitos y estimados usando un modelo simétrico de un material compuesto de capas. Sus influencias sobre la resistencia de propagación de grietas debido a choques térmicos fueron medidas por un ensayo de indentación-temple. Una resistencia altamente mejorada a la propagación de grietas superficiales en las capas exteriores fue encontrada. Los resultados fueron también comparados a otros resultados obtenidos de un material de referencia, un compuesto sin capas, preparado con la misma técnica de fabricación.

Abstract

The microstructure and mechanical properties of an alumina/zirconia functionally graded material prepared by electrophoretic deposition were studied. The microstructure was observed by electron microscopy in order to characterize it with respect to the phases, grains sizes and their distribution. The material had a high quality fine grained microstructure with very little porosity and uniformly distributed ZrO_2 within the layers. The mechanical properties such as hardness, fracture toughness, but mainly residual stresses, arisen as a consequence of thermal expansion coefficients mismatch, were studied by indentation methods. The material exhibited excellent hardness in the exterior layers, comparable to that of pure alumina. The residual stresses were also calculated by utilizing a finite element model and estimated by using a symmetrical model of a layered composite. Their influence on crack growth resistance due to thermal shocks was measured by an indentation-quench test. Highly enhanced resistance in the exterior layers to propagation of surface cracks was found. The results were also compared to those obtained from a reference non-layered composite material, prepared by the same fabrication technique.

Table of Contents

1. Introduction

Functionally graded materials have existed in the nature for a very long time, for example bone and bamboo. The concept has also been exploited for more than thousand years in steel, for example the hardened edge and the tougher interior of knives and swords. However, the research of functionally graded materials had not been very extensive before the late 1980's when Japan launched a national research program on the subject. Since then functionally graded materials have grown to become one of the major current themes in structural materials research. Some examples of target applications that have been proposed over the recent years are: metal to ceramic joining, implants for humans, internal combustion engine components, cutting tools, fire retardants in construction, contact-damage-resistant polymer-matrix composites and rocket thrust chamber linings. Functionally graded materials are also of considerable interest in a variety of non-structural applications where gradients in composition are deliberately introduced to optimise physical properties, for example in optoelectronic devices.

This report deals with the microstructure and mechanical properties of alumina/zirconia functionally graded material prepared by electrophoretic deposition (EPD). Indentations were made to measure hardness, fracture toughness and residual stress. The finite element method and a symmetrical model of a layered composite were also used to calculate the residual stress. Scanning Electron Microscope (SEM) was used to study the microstructure, and the crack propagation behaviour was studied using a thermal shock test. As a help to interpret the test results and to have something to compare with, most of the tests were also carried out on a homogeneous alumina/zirconia composite material.

2. Functionally Graded Materials

2.1. Ceramic Materials

Ceramics are defined as materials that are inorganic and non-metallic. They exhibit useful properties such as high strength and hardness, high melting temperatures, chemical inertness and low thermal and electrical conductivity. However, they have also other, less desirable, properties such as brittleness. The brittleness makes the ceramics very sensitive to defects in the material. It is enough with only one small crack in the ceramics for it to propagate and eventually cause a complete rupture.

The extreme sensitivity to flaws in the material and thus the unreliability in strength has lead to the development of techniques to hinder these cracks to grow, and as a result an increase in strength. One common technique is to introduce toughening mechanisms using platelets, secondary particles, whiskers or fibres. Another well recognised method that has proven inexpensive, and is commonly used in glasses, is the introduction of surface compressive stresses. In ceramics this can be obtained by forming a laminate ceramic composite. That is, to build the material in several ceramic layers of different composition and/or microstructure and stack them on top of each other as shown in figure 2.1.

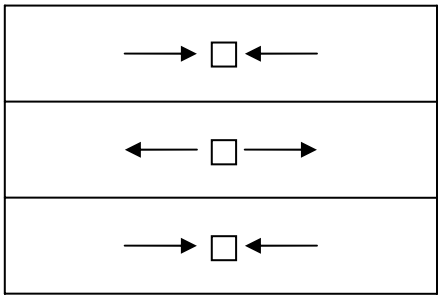

Fig. 2.1 A three layered material with the residual stresses marked with arrows. The interior layer has a higher dilatation coefficient.

Since the layers have different composition and/or microstructure they will also have different thermal expansion coefficients. During the cooling down after the sintering this difference makes these layer materials shrink dissimilarly. The material with higher dilatation coefficient will contract more than the other material. Consequently a residual tensile stress will be formed in this layer and a compressive stress will be induced in the surrounding layers. There is also another source from where the residual stress arises. It is less important and it is the

density difference between materials during sintering [3]. The material that is less dense will contract more and thus induce compressive stresses to the surrounding layers.

The problem with normal multilayer materials is that the layers can have very different composition and properties. Abrupt transitions in these materials' composition and properties often result in sharp local concentrations of stress, whether the stress is internal or applied externally. If these stresses get too powerful the material will crack. In the case that the interface bond is sufficiently strong, the layers experiencing tensile stress might disintegrate, otherwise delamination at the interfaces occurs. The stress concentrations are greatly reduced and better distributed if the transition from one material to the other is made gradual. When sharp interfaces between highly dissimilar solids intersect a free surface, elevated levels of a multi-axial stress-strain field occurs in this region and it is likely that possible cracks nucleate here. Such 'edge effects' can be suppressed and as a consequence the interface bond strength and the damage tolerance are enhanced [13].

By definition functionally graded materials (FGM) are used to produce components featuring engineered gradual transitions in microstructure and/or composition, the presence of which is motivated by functional performance requirements that vary with the location within the part. With functionally graded materials, these requirements are met in a manner that optimises the overall performance of the component [13].

2.2. Alumina, Al_2O_3

Alumina is a popular oxide ceramics with very high hardness and excellent chemical and thermal stability but very low crack growth resistance. Pure fine grained Al_2O_3 powder enables production of a single phase ceramics with regular grain size. Pressureless sintering leads usually to a significant grain growth. To suppress this a little addition of MgO is typically used (usually <0.05 vol%). Without the MgO additive the grain size can reach up to 50 μm. The resulting product may also contain residual porosity but by using a high quality powder this can be reduced down to less than 0.2%. The porosity can be eliminated completely by sintering in a reduction atmosphere (hydrogen). This way a coarse grained translucent or transparent material is formed. For advanced applications, the hot isostatic pressing (HIP) is used by which it is possible to prepare a fine grained (grain size 1-2 μm) fully dense material even without the MgO additives [12].

Al_2O_3 can be found in various crystallographic modifications [15] but in structural applications only α-Al_2O_3, known as corundum, is used. Monocrystallic forms are often called sapphire. α-Al_2O_3 forms by heating of pure alumina in air to the temperatures 1150 – 1300 °C. Its crystallographic structure consists of hexagonal closely packed planes of oxygen anions. In this lattice the aluminium cations, that occupy 2/3 of the octahedral sites, form planes

interlacing the oxygen ions. The basic hexagonal closed packed cell has the dimensions a=0.4759 nm, c= 1.2992 nm. The theoretical density of the α-Al_2O_3 is 3.98 g*cm^{-3}.

Because of its properties, alumina is used in high temperature applications, cutting and abrasive tools, often as a hard coating of a softer substrate.

2.3. Zirconia, ZrO_2

Zirconia, or zirconium oxide, is one of the ceramic materials with the best mechanical properties. It has been traditionally used as a refractory material for its good high temperature properties, but recently its potential as tough ceramics has been appreciated and ways to improve it have been sought. Its recent development enabled use of modern ZrO_2 in applications such as cutting tools for everyday use, or in medicine as material for bone and dental prostheses and implants.

The zirconium oxide can be found in three polymorph modifications: monoclinic, tetragonal and cubic. In the monoclinic form one atom of zirconium is coordinated with seven atoms of oxygen, the dimensions of the crystallographic cell are a=0.5156 nm, b=0.5191 nm, c=0.5304nm, angle β=98.9°, and the density is 5.830 g*cm^{-3}. In the tetragonal form one zirconium atom is coordinated with eight oxygen atoms, and the parameters of the basic cell are a=0.5094 nm, b=0.5177 nm. This phase is the densest, with the theoretical density 6.1 g*cm^{-3}. The cubic phase has a face centred cubic form with cell parameter a=0.5124, and its density is 6.09 g*cm^{-3}. In pure ZrO_2 the monoclinic (**m**) phase is stable up to about 1170°C where it transforms into tetragonal (**t**). At 2370°C the cubic phase forms and remains stable up to the melting point 2680°C. Of these three phases only the tetragonal one entails ceramics with good mechanical properties. In order to maintain this phase at low temperatures various stabilizing additives are used.

The transformation from tetragonal to monoclinic modification is connected with an increase of volume of about 5%, which can be deducted also from the decrease of density. This transformation has diffusionless, martensitic character. If ceramics contains grains of metastable **t**-ZrO_2, these can in the vicinity of propagating cracks, which induces high local tensile stresses, undergo **tetragonal → monoclinic** phase transformation absorbing thus energy and inducing also compressive stresses (due to the volume increase).

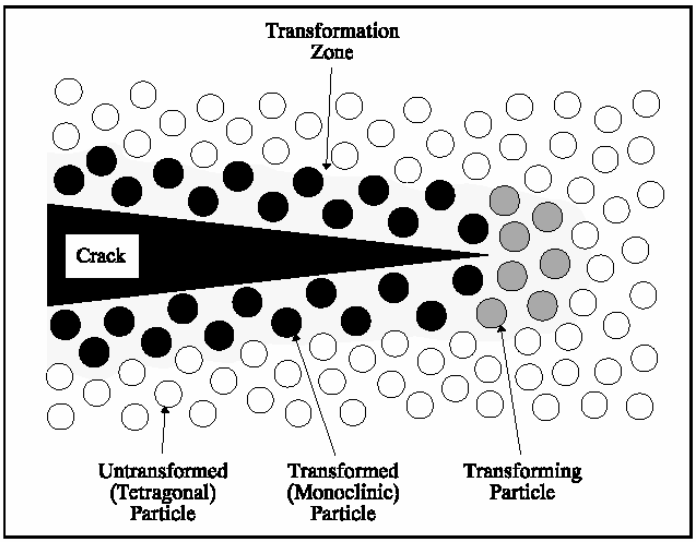

Fig. 2.2 Tetragonal to monoclinic phase transformation [14].

There are several groups of ceramic materials utilizing this phenomenon. They differ in type and amount of the stabilizing additives, fabrication method, and final content of the tetragonal phase. The most frequent are:

(1) Partially Stabilized Zirconia (PSZ), where during heat treatment of cubic ZrO2, stabilized by ~3wt% MgO or CaO, fine coherent t-ZrO2 particles form by precipitation.

(2) Tetragonal Polycrystallic Zirconia (TZP), formed by fine submicron t-ZrO2 grains, stabilized usually by yttria (Y-TZP), but also other stabilizers can be used.

(3) Zirconia Toughened Ceramics (ZTC) where 10-30 wt% of t-ZrO2 grains are dispersed in brittle ceramic matrix such as alumina or mullite.

3. Fabrication

3.1. Fabrication Processes

A wide spectrum of different methods exists to manufacture functionally graded materials [13]. These methods range from well established processes such as those used in case hardening of steel to modern experimental processing methods. Much work to date is focusing on those new processing methods, primarily to find proof of the viability of a given processing route toward FGM production. However, some common trends can be found in this variety of processes, and in particular two classes of methods for the production of FGMs containing a metallic phase can be distinguished.

The first class of production methods is called constructive processes. It wears the name because the FGM is constructed layer by layer in a programmed fashion. This method is attractive because there is no limit on gradients that can be produced.

The second class of production are the transport based processes. They create gradients within a component by natural transport phenomena. These transport based processes use the flow of fluid, the diffusion of atomic species, or the conduction of heat to create gradients in local microstructures and/or compositions. In general, the transport based processes are more cost effective than the constructive processes.

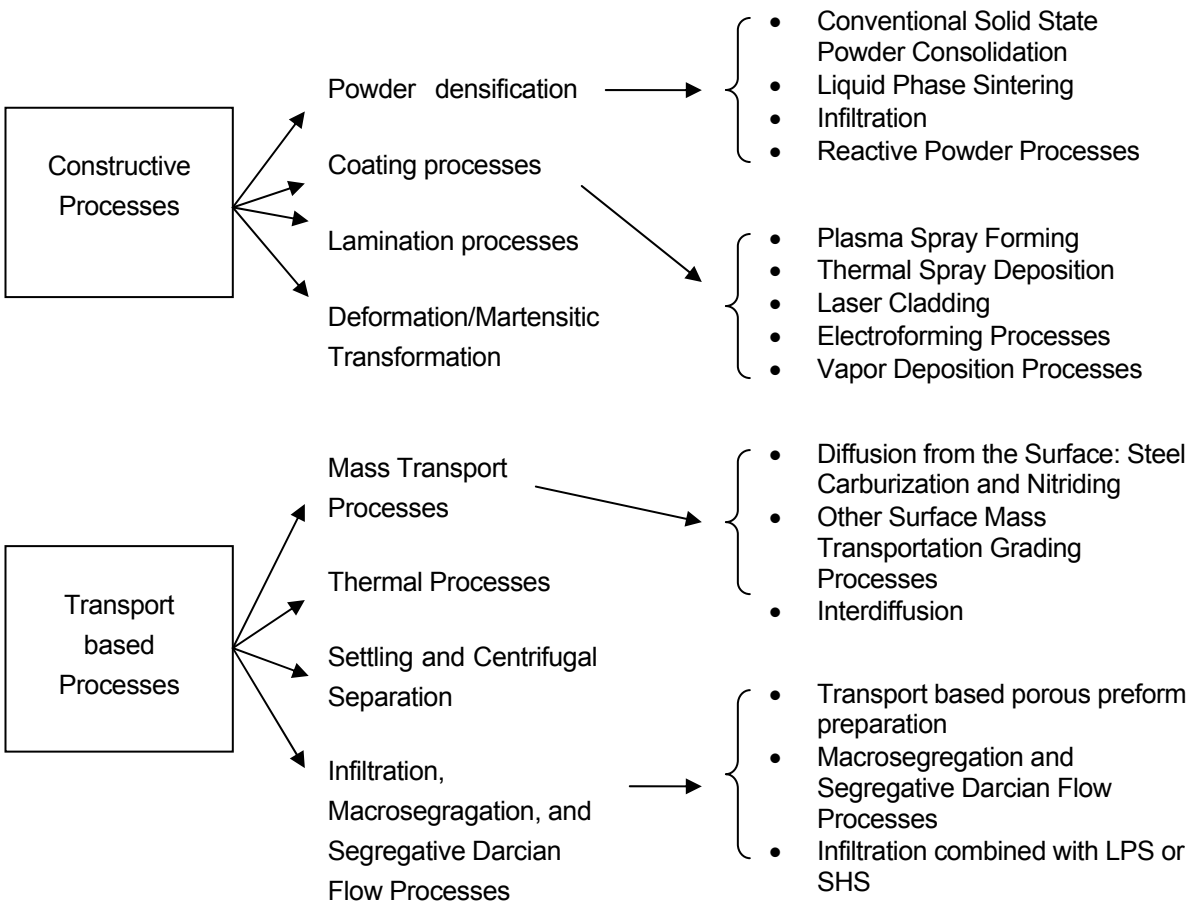

Fig. 3.1 An overview of the different fabrication methods [13].

3.2. Electrophoretic deposition

Electrophoretic deposition from suspensions containing more than one component can be used to produce graded bodies. It takes part of the constructive processes path and is a combination of two processes: electrophoresis and deposition. Electrophoresis is the motion of charged particles in a suspension under the influence of an electric field. Deposition is the coagulation of particles to a dense mass. Electrophoretic deposition is believed to have been used for the first time in 1927 by Harsanyi [4] when he deposited ThO_2 and tungsten on a platinum cathode. One of the advantages of this method is its ability to produce a continuously changing composition without step-wise layers.

The electrophoretic deposition works in such a way that a dc field is used to get the charged particles to move toward, and deposit onto an oppositely charged electrode. In the simplest case an external mixing system supplies a suspension to the deposition cell (for example Al_2O_3). A second suspension is added with time to the mixing system (for example ZrO_2), and as a consequence the composition of the mixing suspension is changed and the material obtains a gradient deposition.

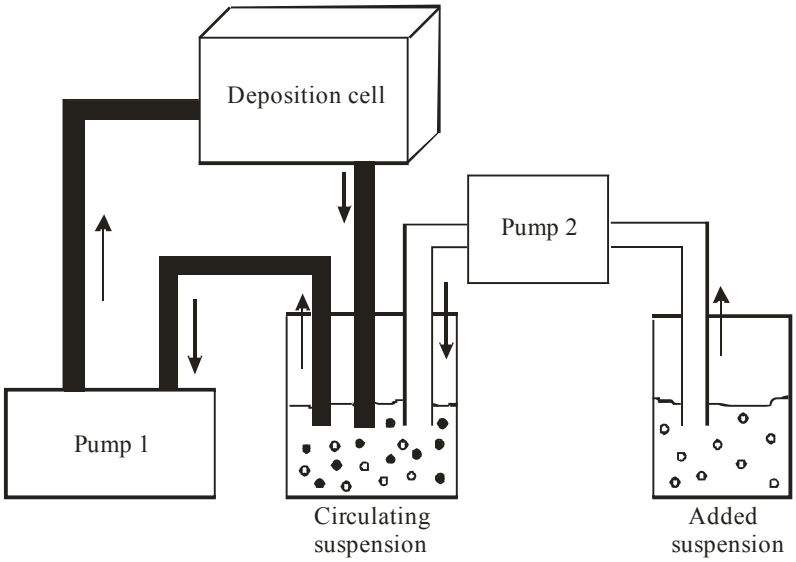

Fig. 3.2 A schematic of the Electrophoretic deposition set-up [7].

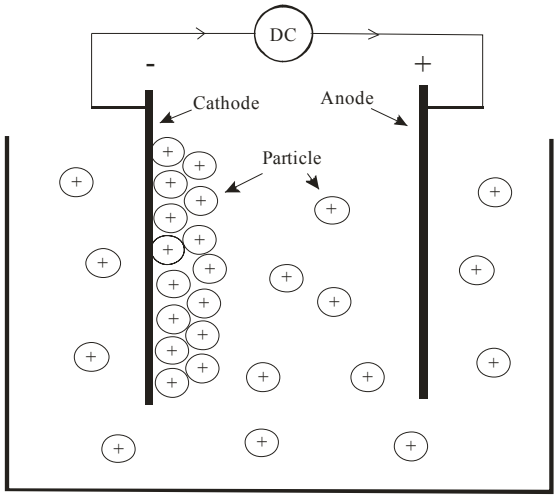

Fig. 3.3 A schematic of the deposition cell [11].

A normal choice of materials is stainless steel for the electrodes and a non conductive material for the recipient and the edges of the electrodes, for example polytetrafluorethylene (PTFE). A graphite coating on the electrodes facilitates the removal of the ceramic material produced. Research has shown that acetone/n-butylamine based suspensions work well with ZrO_2 and Al_2O_3 powders [7].

Another method is to start with one suspension containing both powders of the two materials wanted in the final material [1]. The difference in electrophoretic mobility in the two powders causes one of the powders to deposit faster than the other. The velocity of ceramic particles in suspensions, ν, depends on the electrophoretic mobility μ and the electric field strength E.

$$\upsilon = E\mu \qquad \textbf{(3.1)}$$

The electrophoretic mobility is defined by the properties of the dispersant and the zeta potential of the particles ξ:

$$\mu = \frac{\varepsilon_0 \varepsilon_r}{\eta} \xi \qquad \textbf{(3.2)}$$

where η is the viscosity and $\varepsilon_0\varepsilon_r$ the dielectric constant of the dispersant.

The powder with higher electrophoretic mobility will deposit until there is no more of this powder. As the powder runs out, the other powder will start to deposit and thus resulting in a gradient deposition.

4. Experimental

4.1. Materials

The functionally graded material was an experimental grade manufactured by Katholieke Universiteit Leuven, Belgium. The starting materials were commercially available powders of 3 mol% Y_2O_3 co-precipitated ZrO_2 (Daiichi grade HSY-3U) with an average particle size ~0.3 μm and α-Al_2O_3 (Baikowski grade SM8) with an average particle size ~0.6 μm. As-received powders were ball-milled in ethanol for 24 hours. Electrophoretic deposition (EPD) at a constant voltage was performed in a suspension flow-through deposition cell, where a supply system adds a second suspension to the circulating suspension in the mixing cell at a controlled rate. The process was performed in a way that would in theory lead to a symmetrical configuration of the layered system. The green bodies obtained with the EPD were sintered for 2 hours at 1500°C.

The resulting material was supplied in form of discs approximately 4 mm thick and with the diameter 36 mm. The discs were formed by three layers with gradient transitions between them. The two exterior layers consisted of a homogeneous mixture of 90% Al_2O_3 and 10% ZrO_2, whereas the inner layer consisted of a homogeneous mixture of 70% Al_2O_3 and 30% ZrO_2. The disc was delivered slightly curved in a concave manner due to contractions during the cooling process.

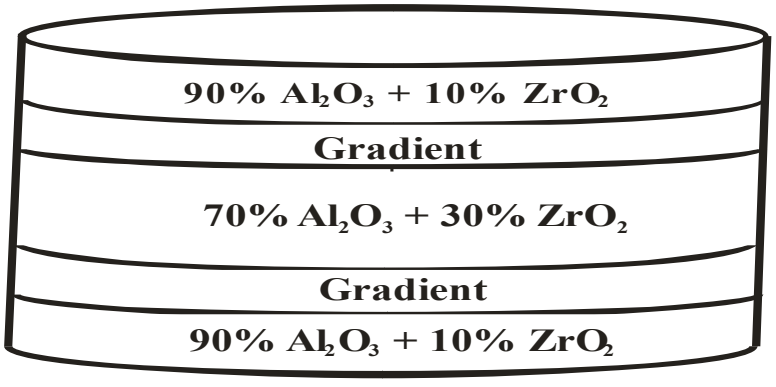

Fig. 4.1 Sketch of the gradient material

Another material was also used in some of the tests as a comparative specimen. This material will be referred to as the homogeneous material since it consisted of a homogeneous mixture of 90% Al_2O_3 and 10% ZrO_2 and no gradient. This material was also in the form of a disc with the same dimensions as the material mentioned above.

It is difficult to say for sure the real values of the dilatation coefficient, elasticity modulus and density for all configurations present in our system. For that reason their values for the range of compositions were estimated by the linear rule of mixture using the experimental values of Sbaizero and Lucchini [9] and the values of Marqués [5]. The following approximate values have been used for the residual stress estimations.

Table 4.1 Properties of the homogeneous layers of the graded material.

	Inner layer 70% Al_2O_3 + 30% ZrO_2	Outer layer 90% Al_2O_3 + 10% ZrO_2
Density	4.53 g/cm^3	4.11 g/cm^3
Dilatation expansion coefficient	10.20 * 10^{-6} K^{-1}	8.99 * 10^{-6} K^{-1}
Elasticity modulus	318 GPa	373 GPa
Poisson's modulus	0.278	0.266

4.2. Sample preparation

The two discs were cut into smaller bars with the dimensions approximately 25*4*4 mm^3. After the cutting, the cross sections faces of the specimens were ground and polished using SiC polish paper for the coarser grinding and subsequently polishing clothes impregnated by diamond pastes were used. Diamond pastes with grain sizes down to 1 μm were used for the gradient material, and for the homogeneous material diamond pastes with grain sizes down to 6 μm were used.

4.3. Microstructure study

A Scanning Electron Microscope (SEM) was used for studying the microstructure of the functionally graded material. The SEM is an extremely useful tool for this purpose. It works in such a way that the surface of the specimen is scanned by an electronic beam, and the reflected, or back scattered, beam is then collected and displayed at the same scanning rate on a cathode ray tube. The image that appears on the screen represents the surface. The surface may or may not be polished and etched but it must be conductive. If the material is not conductive a very thin metallic or other conductive layer must be applied, normally gold or carbon is used. Scanning Electron Microscopes have very large depths of focus and their useful magnifications range from 100 to 20,000X. The elemental composition of very localized surface areas is possible with the help of accessory equipment.

The SEM observations were carried out on the graded material using a JSM 6400 scanning electron microscope equipped with a microanalytical unit LINK (by Oxford Systems Ltd) for chemical analysis by means of X-ray energy dispersive spectrometry (EDS).

The cross section surfaces were prepared by careful diamond polishing and were thermally etched at 1400°C for 1 hour in order to reveal the microstructure. Finally before observation they were coated by a thin layer of gold.

The EDS was used to identify constituents, and to observe and measure the actual dimensions of individual layers. In order to visualize this, the elements mapping and line scan techniques were used.

4.4. Hardness

Hardness is a measure of the material's resistance to deformation. Besides measuring the hardness, simple normal indentation provides a basic tool for approximately gauging the resistance of surfaces to contact damage, impact or penetration.

Vickers hardness measurements were carried out using a standard indentation machine, Frank 532. The sizes of the indents were measured by an optical microscope connected to a computer equipped with the software Motic Images Advanced 3.0, by Micro-Optic Industrial Group Co, Ltd.

In the case of the functionally graded material the indentations were made in lines across the polished surface transversal to the composite layers. The indentations were aligned so that their diagonals and radial cracks were parallel and transversal to the composite layers. The idea was to get a hardness profile throughout the specimen for comparison of the layers as well as the intermediate graded layers. Three different loads were used: 3 kg, 5 kg and 10 kg. A total of 33 indentations were carried out on the graded specimen. Consideration was taken to the distances between the indentations so that they would not affect the results of the neighbouring indentations.

In the case of the homogeneous material the indentations were carried out randomly throughout the specimen, although not compromising on the distance between the indents to guarantee that correct values were obtained. Two different loads were used: 5 and 10 kg. A total of 8 indentations were carried out on the homogeneous specimen.

The hardness values (H) were calculated using the standard formula:

$$H = \frac{1.8544F}{d^2} \qquad \textbf{(4.1)}$$

where F denotes the indentation load, d is the length of the indentation impact diagonal calculated in each case as an average value from both diagonals.

4.5. Fracture toughness

When Vickers indentations are made in a brittle material such as ceramics, cracks propagate from each of the four corners of the indentation. By measuring the length of the parallel half crack produced, the crack propagation resistance i.e. the fracture toughness K_{IC} can be obtained using the following formula [6]:

$$K_{IC} = \frac{\eta F \sqrt{\frac{E}{H}}}{c^{3/2}} \qquad \textbf{(4.2)}$$

where η is a geometric factor, E is the modulus of elasticity, c is the indentation radial crack half-length at the surface. The term $\eta\sqrt{(E/H)}$ was approximated to the value 0.07, which is a typical value for alumina ceramics. Only the cracks parallel to the layers were used as these are not so influenced by the residual stresses in the layer plane. In the case of the homogeneous material the mean values of the parallel half cracks and the transversal half cracks were used instead of only the parallel half crack values because they were not subjected to residual stresses.

All values of the fracture toughness (K_{IC}) were calculated from the cracks produced from the hardness indentations described above.

4.6. Residual stress

4.6.1. Residual stresses measured by indentation crack lengths

Residual stress is the stress that persists in a material that is free of external forces and temperature gradients.

On a stressed surface the equilibrium length c_R of the indentation cracks is determined by the critical stress intensity factor, i.e. the fracture toughness.

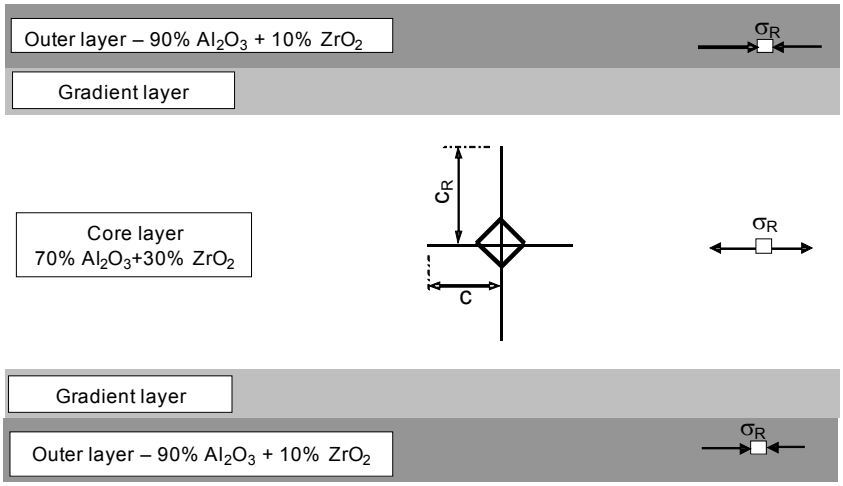

Fig. 4.2 Scheme of the graded material with an indentation and the accompanying parallel and transversal cracks, as well as the residual stresses

The fracture toughness corresponds to a sum of the actual stress intensity factor K_I originating from the deformation zone introduced by indentation and K_R from the residual stresses:

$$K_{IC} = K_I + K_R \qquad \textbf{(4.3)}$$

This in plane residual stress intensity factor can be expressed:

$$K_R = Y\sigma_R c_R^{1/2} \qquad \textbf{(4.4)}$$

where Y is a geometric constant (~1.26) and σ_R is the residual stress. It is assumed that the residual stress is constant along the crack path even if in the gradient part it obviously cannot be the case. However, by taking in account the whole crack an estimation of the average value of the residual stress in the centre of the indentation can be made.

The value of the residual stress is therefore given by:

$$\sigma_R = \frac{K_{IC} - K_I}{Yc_R^{1/2}} = \frac{K_{IC}\left[1 - \left(\frac{c}{c_R}\right)^{3/2}\right]}{Yc_R^{1/2}} \qquad \textbf{(4.5)}$$

if $\sigma_R > 0$ the stress is tensile

if $\sigma_R < 0$ the stress is compressive

4.6.2. Residual stresses calculated by a non gradient laminate model

The residual stress was not only measured, but also estimated by a simple symmetrical layered structure as shown in figure 4.3. The residual stresses that arise in a non gradient multi layer material due to thermal expansion coefficient mismatch are here derived:

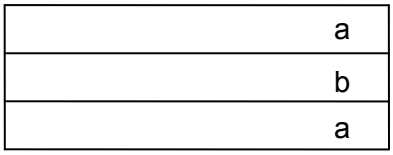

Fig. 4.3 Non-graded multi layer material with the layers marked ‘a’ and ‘b’.

Consider **n** number of layers **a** with thickness $\mathbf{t_a}$, and (**n-1**) number of layers **b** with thickness $\mathbf{t_b}$.

The elastic stresses are according to Hooke´s law:

$$\sigma_a = \varepsilon_a E_a \qquad \textbf{(4.6)}$$

$$\sigma_b = \varepsilon_b E_b \qquad \textbf{(4.7)}$$

where σ is the residual stress and E is the elastic modulus.

$$\Delta\varepsilon = \int_{T_1}^{T_2} (\alpha_a - \alpha_b) dT \qquad \textbf{(4.8)}$$

where T_1 is the current temperature and T_2 is the processing temperature.

For forces in equilibrium the following can be stated:

$$\varepsilon_a E_a n t_a + \varepsilon_b E_b (n-1) t_b = 0 \qquad \textbf{(4.9)}$$

then from equation 4.9:

$$\varepsilon_a = \frac{\Delta\varepsilon E_b (n-1) t_b}{E_a n t_a + E_b (n-1) t_b} = \frac{\Delta\varepsilon}{1 + \dfrac{E_a n t_a}{E_b (n-1) t_b}} \qquad \textbf{(4.10)}$$

$$\varepsilon_b = -\frac{\Delta\varepsilon E_a n t_a}{E_a n t_a + E_b (n-1) t_b} = -\frac{\Delta\varepsilon}{1 + \frac{E_b (n-1) t_b}{E_a n t_a}} \quad \textbf{(4.11)}$$

The residual stresses are then given by:

$$\sigma_a = \frac{\Delta\varepsilon E_a}{1 + \frac{E_a n t_a}{E_b (n-1) t_b}} \quad \textbf{(4.12)}$$

$$\sigma_b = -\frac{\Delta\varepsilon E_b}{1 + \frac{E_b (n-1) t_b}{E_a n t_a}} \quad \textbf{(4.13)}$$

4.6.3. Residual stress by the finite element method (FEM)

Since the calculations above are specifically for non graded multi layer materials, the residual stresses were also estimated with the finite element method.

The finite element method is a numerical analysis technique for determining approximate solutions to a wide range of engineering problems. Its advantages are foremost its ability to replace tests on real specimens that might be very expensive and time consuming to carry through.

The software Abaqus (version 6.4-1) was used to make a model of the residual stresses that was formed during the sintering. The layer thicknesses were modelled according to the values measured with the SEM. A two dimensional rectangular model was created with the mesh dimensions 83 * 72, in direction 1 and 2 respectively (fig. 4.4). In direction 2, the outer layers consisted of 11 meshing rectangles each. The two gradient sections consisted of 25 rectangles each and the core material consisted of 11 rectangles. The specimen was fixed in direction 2.

All the values used in the model for the elements inside the gradient parts, which were not available in literature, were calculated from the properties in Table 4.1, using the linear rule of mixture.

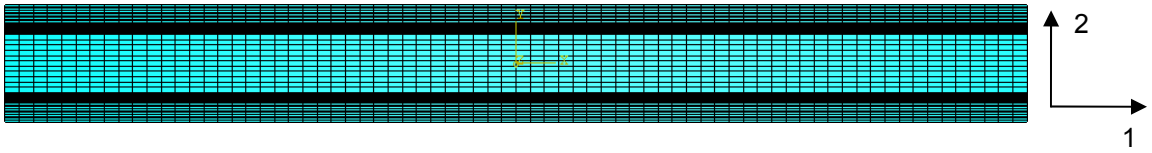

Fig. 4.4 The mesh created with Abaqus.

In the simulation the temperature passed from 1500°C down to 25°C. The stresses in direction 11 were examined. The procedure has been described more in detail in the work of Marqués [5].

4.7. Thermal shock

Graded materials, which are being considered for use in thermal barrier coatings and in engines for supersonic and space vehicles are generally subjected to thermal shock (i.e. rapid changes in temperature which engender spallation and cracking). The aim of this test was to subject the specimen to great stresses and see what would happen with the cracks. How much they would grow, how they would grow etc.

The indentation-quench method was chosen because of its simplicity and low cost. It is also a test that is rather low time consuming. According to P. Pettersson et al. [10] this method allows the use of one specimen throughout the test, whereas other methods as for example the quench-strength method requires a whole set of specimens.

Nine indentations were made in the homogeneous specimen and twelve indentations were made in the layered composite in order to introduce pre-cracks (fig. 4.5). Eight of the twelve indentations were made in the exterior layers and the remaining four indentations were carried out on the interior layer. The pre-cracks are essential because they are much larger than already existing cracks, and therefore statistically distributed cracks can be ignored. All indentations were made with a 3 kg load so that the pre-cracks would have approximately the same length.

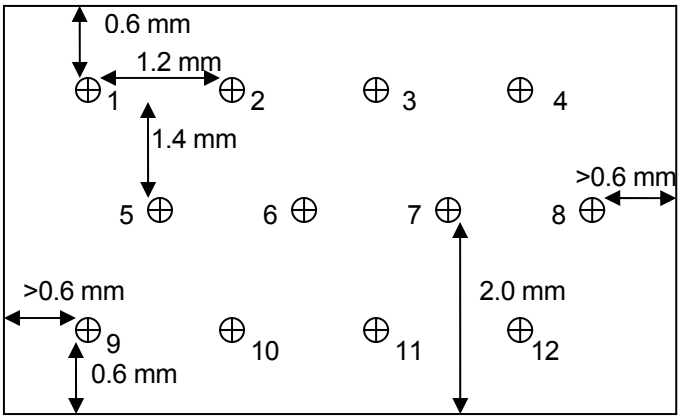

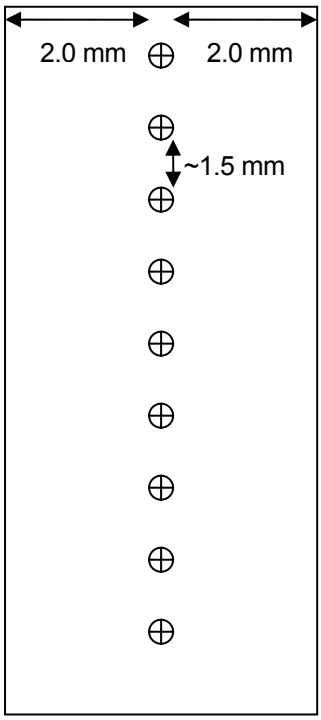

Fig. 4.5a The gradient material with its 12 indentations and the distances between them (above). **b** The homogeneous material with its 9 indentations and the distances between them (right).

The lengths of the cracks were measured with the same equipment as in the hardness and fracture toughness tests. After that the specimens were heated up in a laboratory furnace Obersal HD-230 to a specified temperature and held there for 25 to 30 minutes in order to assure temperature uniformity before quenching. Then the specimens were rapidly put into a 25 degrees Celsius water bath. After this the cycle was repeated; new measurements of the crack lengths were carried out, a heating up to a higher temperature was performed and finally the rapid cooling down into the water bath.

The following temperatures were used in the above described thermal shock cycles:

The graded material: 200°C, 250°C, 300°C, 350°C and 400°C.

The homogeneous material: 150°C, 200°C, 250°C, 300°C, 350°C and 400°C.

5. Results and discussion

5.1. Microstructure

The pictures beneath show the images taken with the Scanning Electron Microscope.

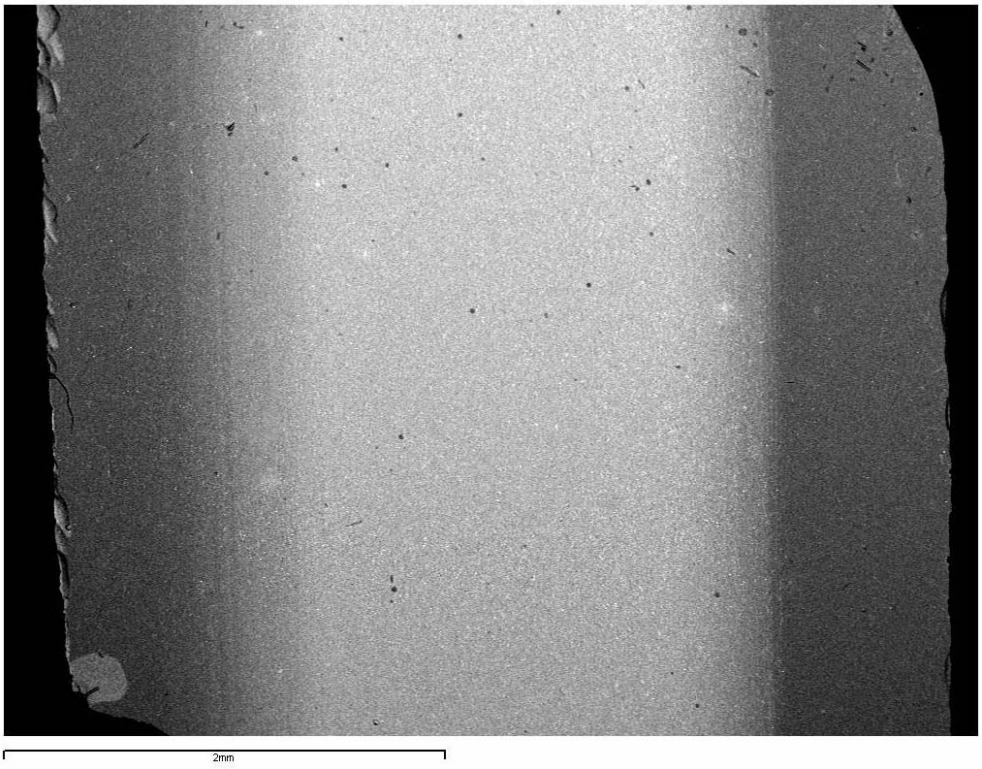

Fig. 5.1 Overall view of the polished cross section showing the layered structure of the alumina-zirconia composite with three thicker homogeneous layers separated by thinner compositionally graded intermediate layers.

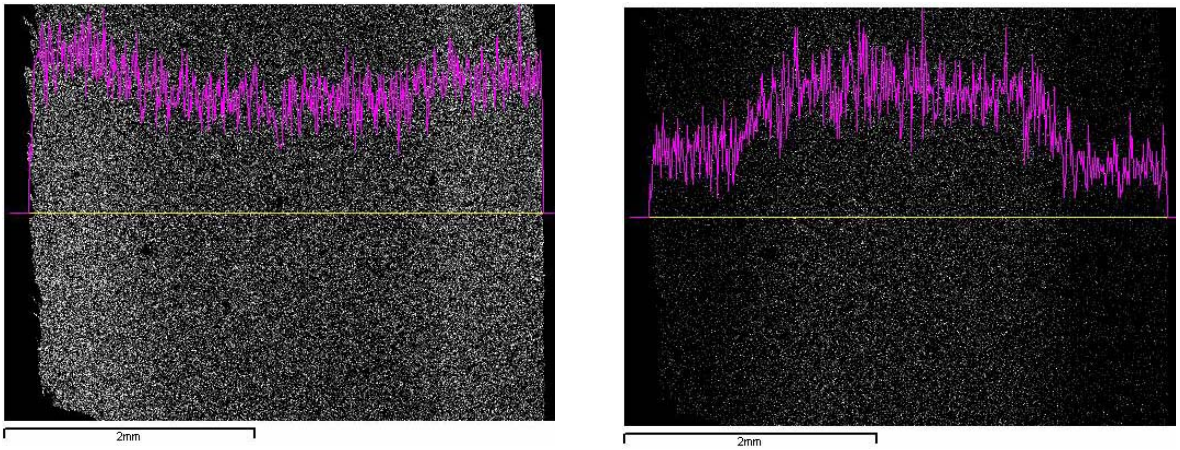

Fig. 5.2a,b Changes of the relative contents of aluminium (a) and zirconium (b) from one edge to the other.

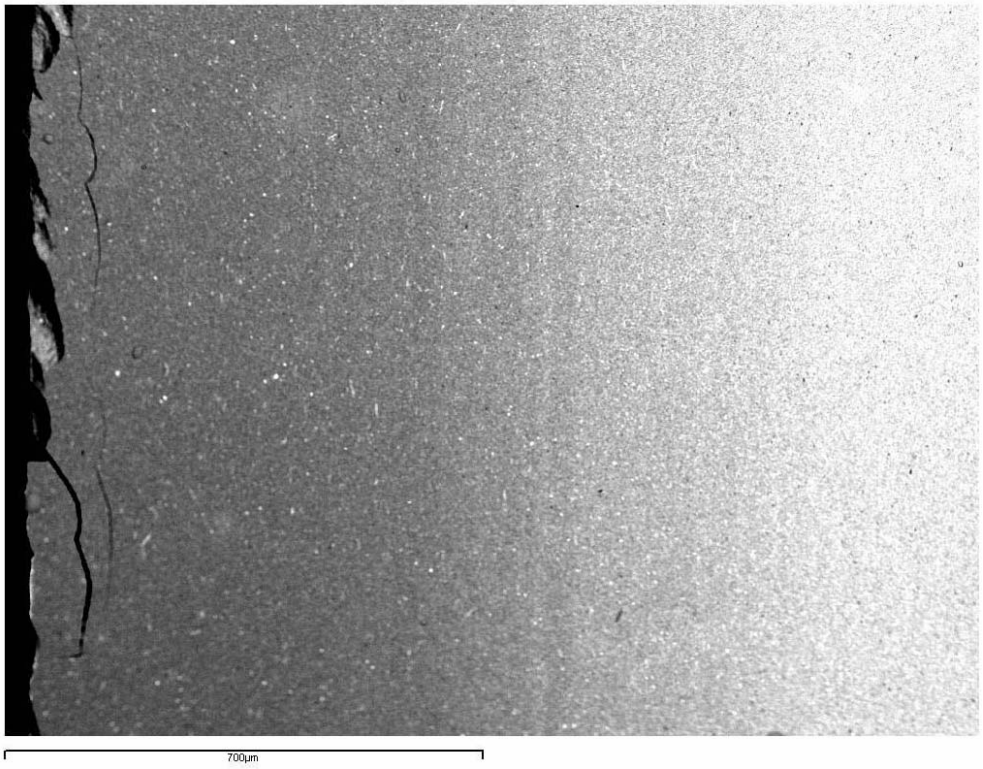

Fig. 5.3 Magnified view of a gradient layer.

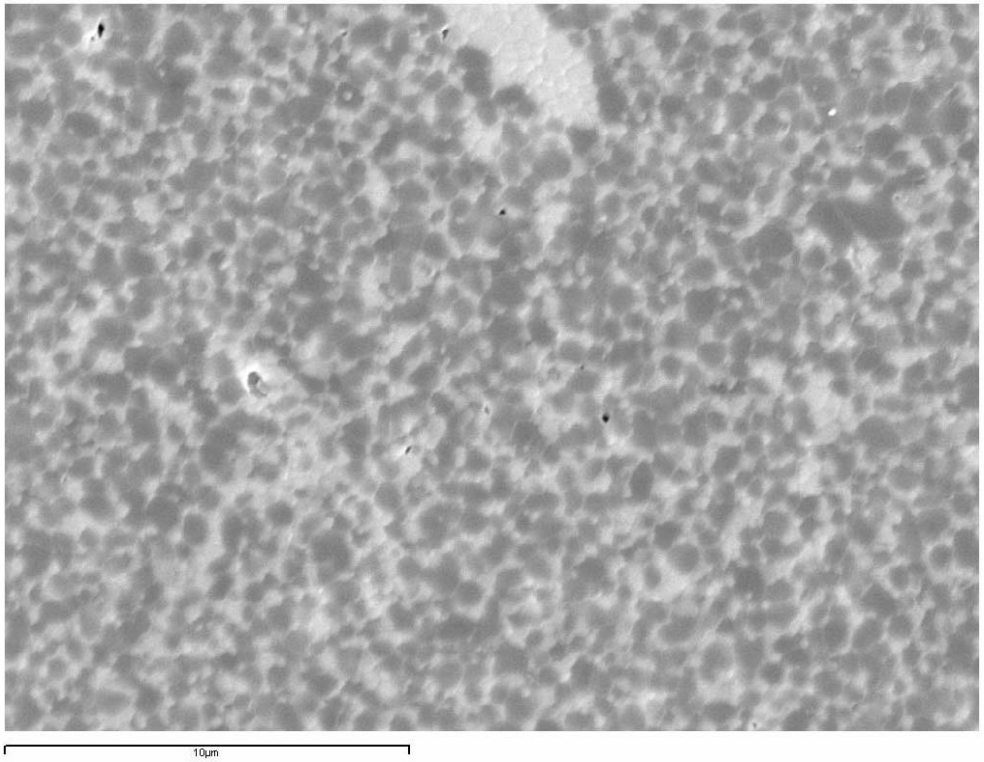

Fig. 5.4a Detail of the microstructure in the central homogeneous layer with high ZrO_2 content.

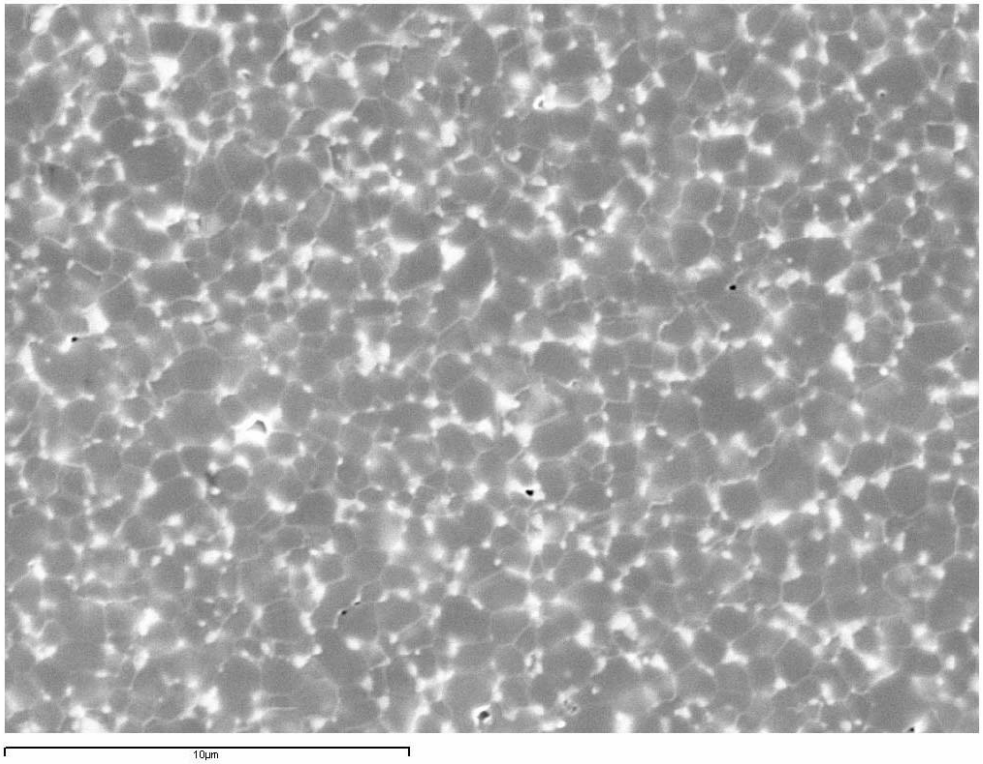

Fig. 5.4b The microstructure of one of the exterior homogeneous alumina-zirconia layers.

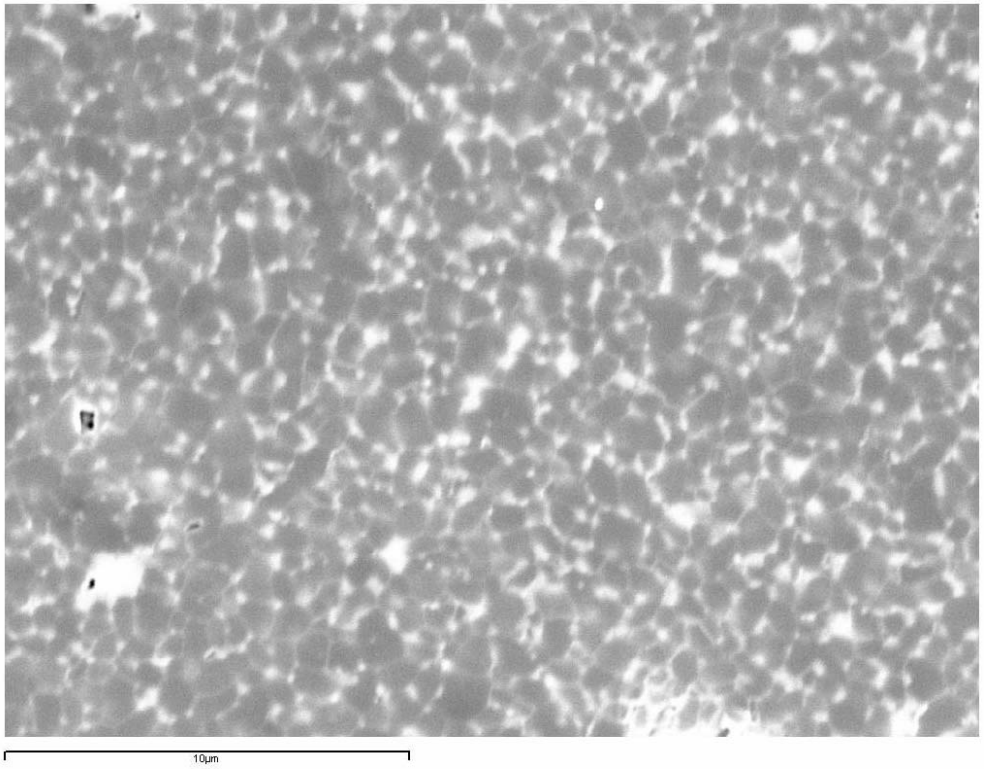

Fig. 5.4c The microstructure of one of the exterior homogeneous alumina-zirconia layers (the opposite side of that in the figure 5.4b above).

Figure 5.1 is a SEM micrograph of a polished and thermally etched surface of the layered composite cross section, showing the compositional changes in the different layers. As expected, there are three homogeneous layers containing 10 vol% zirconia, 30 vol% ziconia (centre) and again 10 vol% zirconia, separated by thinner compositionally graded intermediate layers. The figures 5.2a,b show the complementary EDS maps illustrating changes of relative contents of the Al and Zr, respectively. The gradual transition from outer to central layer can be observed more in detail in figure 5.3.

The figures 5.4 show SEM micrographs of a polished and thermally etched surface for each homogeneous layer, showing the grain sizes and the distribution of both principal phases. In the central layer (Fig 5.4a), apart from homogeneously distributed zirconia (bright grains), occasionally zirconia agglomerates or grain chains can be seen. This can be deleterious for the mechanical stability of the composite, as we can expect higher thermal residual stresses in the vicinity of zirconia agglomerates. The martensitic transformation into monoclinic phase of lower density, associated with the expansion of zirconia grain and the subsequent creation of microcracking is more likely to occur in bigger grains.

Generally, it can be seen, that the microstructure was well formed throughout the whole material. In the central layer it consisted of equiaxed alumina matrix grains with an average

size of 0.5 – 0.9 μm and smaller homogeneously distributed zirconia grains with sizes between 0.2 μm and 0.4 μm. The zirconia grain clusters reached sizes up to 8 μm. The presence of zirconia effectively inhibited the alumina grain growth which can be demonstrated by the fact that in the outer layers (fig. 5.4b,c) with lower zirconia contents the alumina grains had typically sizes from 0.7 μm up to 1.5 μm. The grain growth blocking is normally a desirable property since smaller grains imply better strength in the material, but in cases where one prioritizes the creep resistance or fracture toughness, larger grains are eligible. The figures 5.4b,c indicate that the exterior layers had very similar microstructures.

In all layers only very little porosity was observed, and also this seemed to be mostly due to the grain pull-out during polishing rather than a real feature of the microstructure. The conclusion can be drawn that a satisfactorily dense microstructure had been achieved in the material.

The SEM study also allowed measuring of the dimension of each layer, as they were not exactly known because of the nature of the EPD fabrication method. Without this knowledge it would not be possible to calculate the residual stresses correctly. As it turned out, the material was not completely symmetrical, but this deviation from symmetry was rather small. The layers thicknesses were as indicated in figure 5.5.

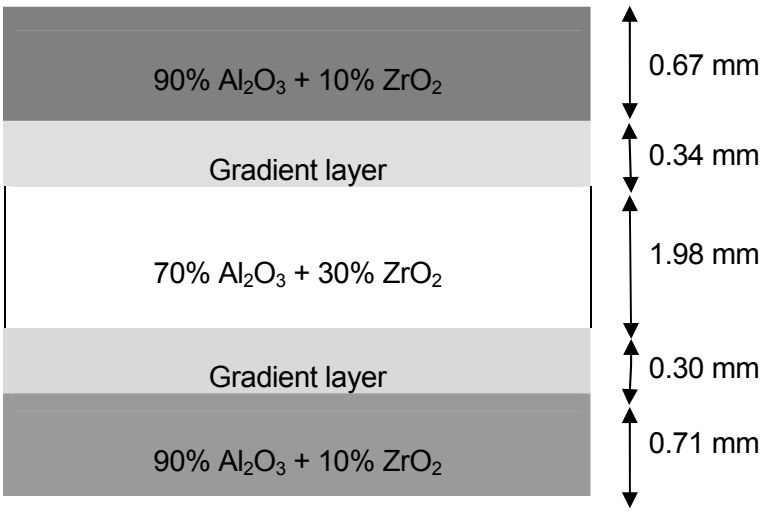

Fig. 5.5 The layer thicknesses in the graded material.

These small differences in layer thickness could explain the slight curved character of the supplied disc.

5.2. Hardness

The results of the hardness measurements for the graded material are shown in the figure 5.6. As expected it is clearly shown that the material closest to the edges was harder than the core material. This is a property that is wanted, because a harder surface implies a better contact damage resistance. The harder outer layers are due to the fact that alumina is a harder material than zirconia and that the composition of the exterior layers is 90% Al_2O_3 and 10% ZrO_2 whereas the core layer contains only 70% Al_2O_3 and 30% ZrO_2.

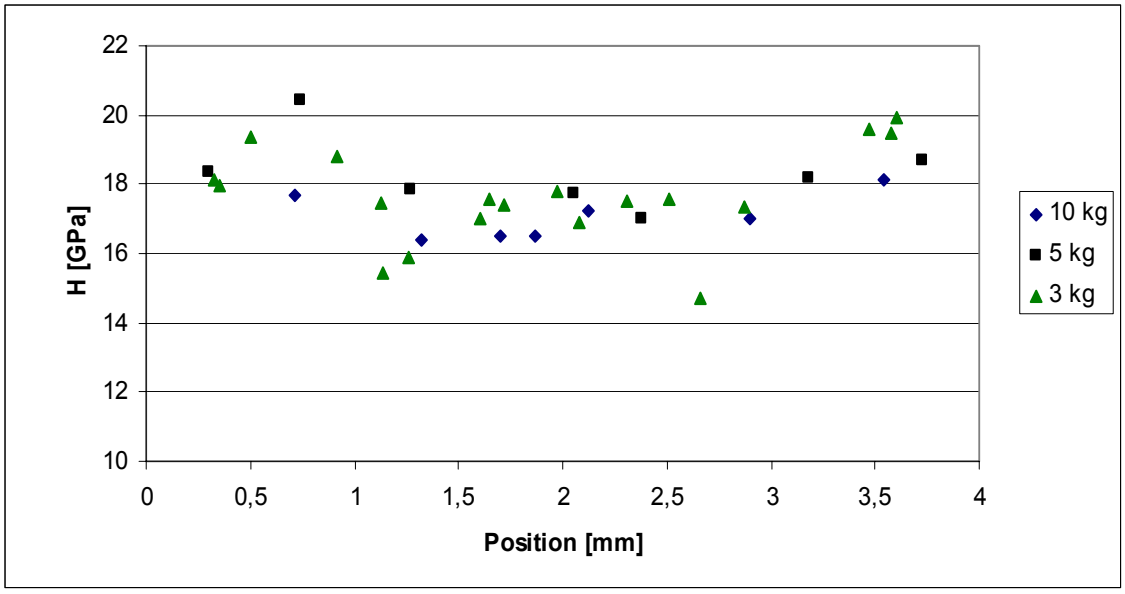

Fig. 5.6 Hardness of the graded material as a function of the distance from one edge to the other.

The highest hardness values measured were around 20 GPa, whereas the lowest values were around 16 GPa. These results are in a good agreement with literature data for technical ceramics [12]. Actually the hardness of the exterior layers exhibits values more typical for monolithic alumina (18-20 GPa [12], 17-18 GPa [2]) which can be attributed to the very dense, fine grained matrix, whose hardness had not been significantly decreased by the zirconia addition. The hardness of the central layer was comparable to that of alumina + 15vol% zirconia composite (15-16 GPa) studied in [2], a material with analogous compositional and microstructural characteristics. Again, considering higher zirconia contents, the present values are slightly higher, but the material in the work [2] seems to contain more microdefects than the EPD composite studied in this work.

In the case of the homogeneous specimen the nine indentations had the mean and median value 17 GPa. The relatively lower value, when compared to the corresponding layer in the

FGM, can be a result of the quality of the polished surface, which perhaps in this case was not as good.

5.3. Fracture toughness

Figure 5.7 shows the fracture toughness measurements for the graded material. As expected the fracture toughness is higher in the central layer that contains 20 volume percentage units more of the tougher zirconia than the outer layers.

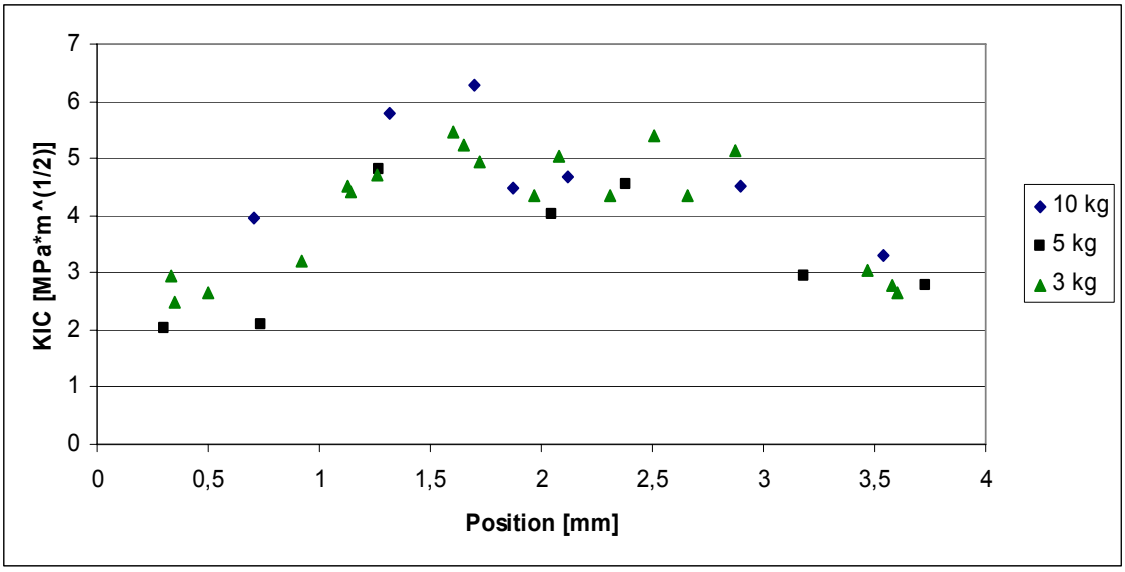

Fig. 5.7 Fracture toughness of the graded material as a function of the distance from one edge to the other.

The highest fracture toughness values were about 5.5 - 6 MPa*m$^{1/2}$, whereas the lowest values were found to be 2 - 2.5 MPa*m$^{1/2}$. For the homogeneous specimen the mean and median values were 4.6 MPa*m$^{1/2}$.

The literature data for analogous homogeneous alumina/zirconia composite [2] range from 4.5 to ~5 MPa.m$^{1/2}$ depending on the grain sizes. In this study the results tend to be a little lower, only the central part containing 30vol% ZrO_2 is tougher. However this can be simply due to the fact that the authors of [2] used a particularly calibrated value of the material constant η from the equation 4.2 which was about 50% higher than the standard value used in this work.

Although no specific R-curve behaviour observation was performed (rising crack propagation resistance with crack growth), it seems that no particular trend in K_{IC} with respect to the indentation load was apparent. If some toughening takes place it is probable that the

saturation crack length is rather short and that the effective K_{IC} stays the same for all indentation loads used in this test.

5.4. Residual stresses

5.4.1. Measured

The residual stresses calculated from the indentation cracks are shown in figure 5.8. The exterior layers are subjected to compressive stresses of about 200 MPa while the interior layer is subjected to tensile stresses with a maximum of about 240 MPa. No sharp stress transitions exist and only low values of the residual stresses are found in the graded sections, showing that the theory of lowering stress concentrations by introducing graded transitions works very well.

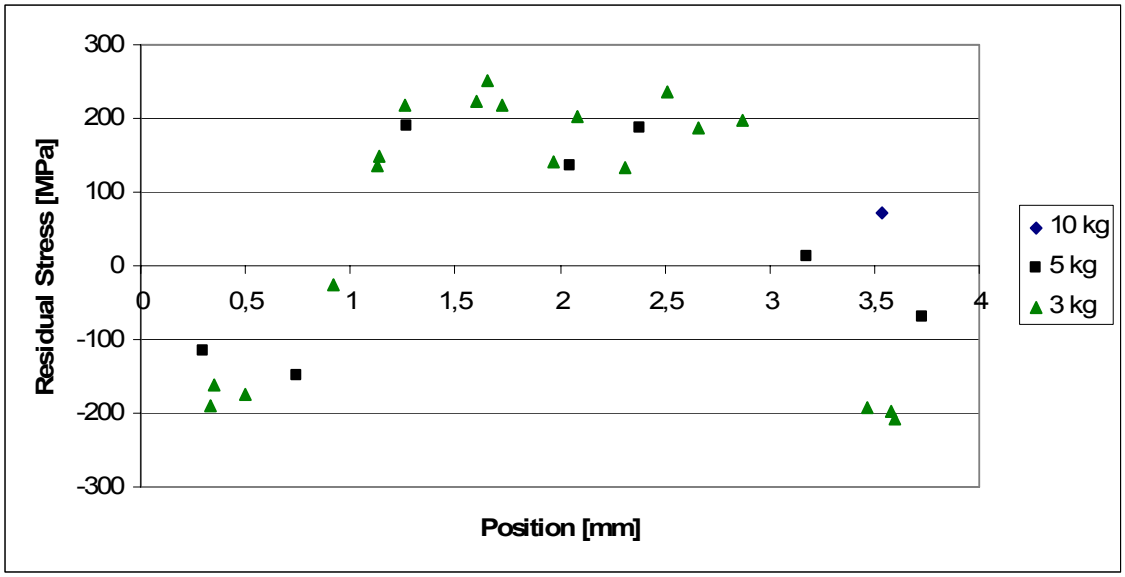

Fig. 5.8 Residual stress in the graded material as a function of the distance from one border to the other.

5.4.2. Non-gradient laminate model

Since the gradient layers were relatively thin when compared to the homogeneous ones, the material could be approximated by a simple layered structure as it is described in chapter 4.6.2. Using the values of the material properties from Table 4.1, and the following input data:

n = 2 layers

t_a = 0.69 mm (the mean value of the two exterior layers)

t_b = 1.98 mm

T_1 = 25°C

T_2 = 1500°C

The residual stresses were calculated by means of the equations (4.12) and (4.13). The highest tensile stress (σ_b) was 255 MPa and situated in the core layer whereas the highest compressive stress (σ_a) was 366 MPa and located in the exterior layers.

5.4.3. Finite element method

The exact compositional profiles of the graded layers were not possible to obtain because of their relatively small thicknesses and the EDS limitations during SEM analysis. Therefore it was assumed that the gradients had a linear character. It was further assumed that that no tetragonal-to-monoclinic transformation of zirconia took place during cooling. No study (e.g. X-ray diffractography) to identify all zirconia allotropes in the system was carried out, but in the work of M. Popa et al. [8] the authors studied a very similar FGM material produced by the same fabrication method. Apart from the tetragonal phase they did not find any other ZrO_2 phase.

The residual stresses calculated with the finite element method are shown in figure 5.9 and 5.10. The values presented later on were estimated in the centre of the specimen along axis 2, where no edge effects were present.

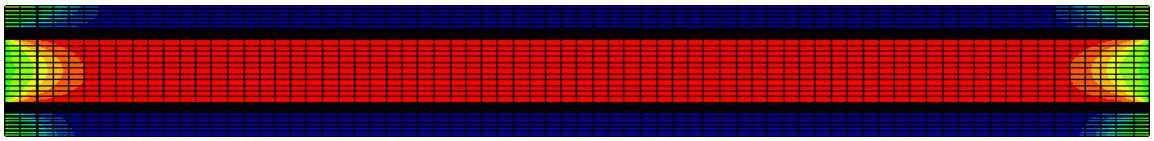

Fig. 5.9 Picture of the whole FEM specimen to illustrate the range of the edge effects.

The highest tensile stress was 269 MPa and situated in the core layer. The highest compressive stress was 364 MPa. These values are very close to the values calculated by the simple layered model. The reason for this is that the gradient layers were relatively thin when compared to the homogeneous ones.

The small discrepancy from symmetry of layer thickness of the specimen did not give rise to any apparent differences in residual stress.

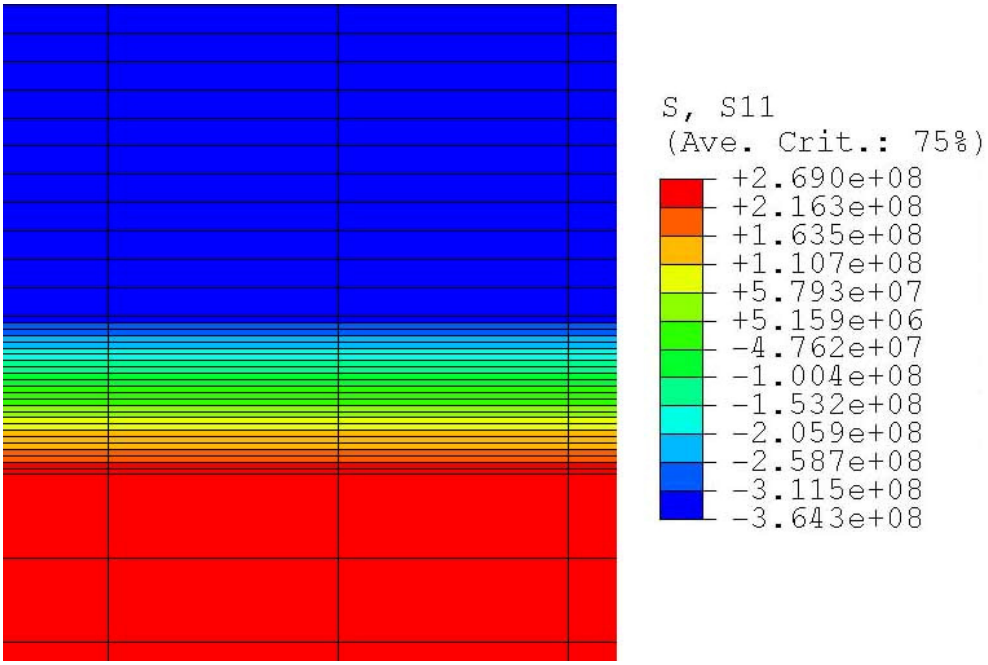

Fig. 5.10 FEM model of the graded material. The image shows a piece of the upper half of the specimen, the blue colour is where the exterior layer is situated. The red colour is where the interior layer is situated. The values are given in Pascal.

The two models gave higher residual stresses than the indentation measures of the specimen. They present about 165 MPa higher maximum compressive stresses and about 20 MPa higher maximum tensile stresses than the empirical measures. The reason for the differences is that the theoretical calculations are based on a perfect material, which is not the case in the specimen. In reality the high internal stresses may be relieved by some residual porosity, by deformation and/or transformation processes, and also by the sectioning of the specimens, which creates free surface that is not considered in the model.

5.5. Thermal shock tests

The figures 5.11 - 5.17 show the results of the thermal shock tests. Note that the maximum crack length marked out is 300 µm. Larger crack lengths or unstable cracking (cracking to the edges or into other indentations) are not marked out in the figures. For better visibility in the photographs, the surfaces were after the tests impregnated with a penetrating dye. Firstly it should be noted that the error margin is quite large in this test due to difficulties to see the cracks at all time in the magnifier. Nevertheless, some trends can clearly be observed.

Secondly it can be noted that the produced cracks in the parallel directions and the cracks in the transversal directions did not have the same lengths directly after the indentations, even if

they were in the same layer. This is due to the effects of the earlier mentioned compressive and tensile stresses which either facilitates the propagation of cracks or make them propagate more difficultly.

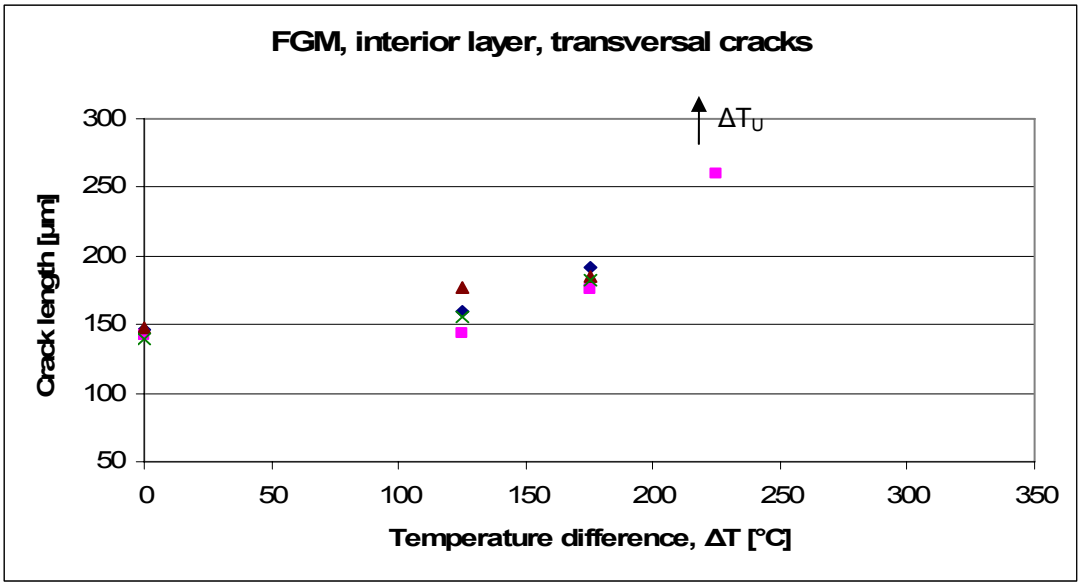

Fig. 5.11 Crack propagation of the transversal cracks in the inner layer of the graded material as a function of temperature difference. The temperature difference for unstable cracking is shown with an arrow.

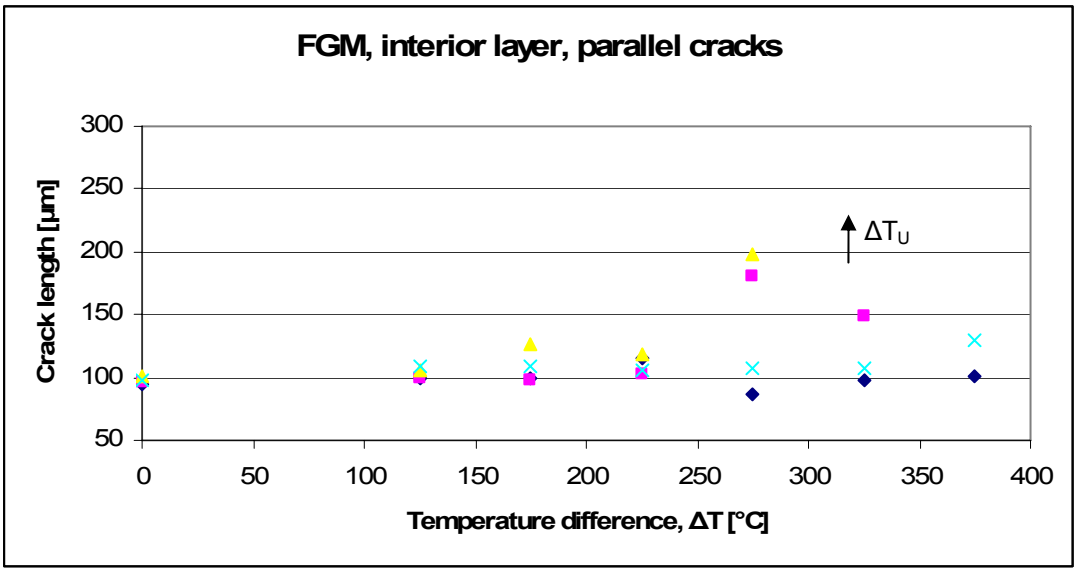

Fig. 5.12 Crack propagation of the parallel cracks in the inner layer of the graded material as a function of temperature difference. The temperature difference for unstable cracking is shown with an arrow.

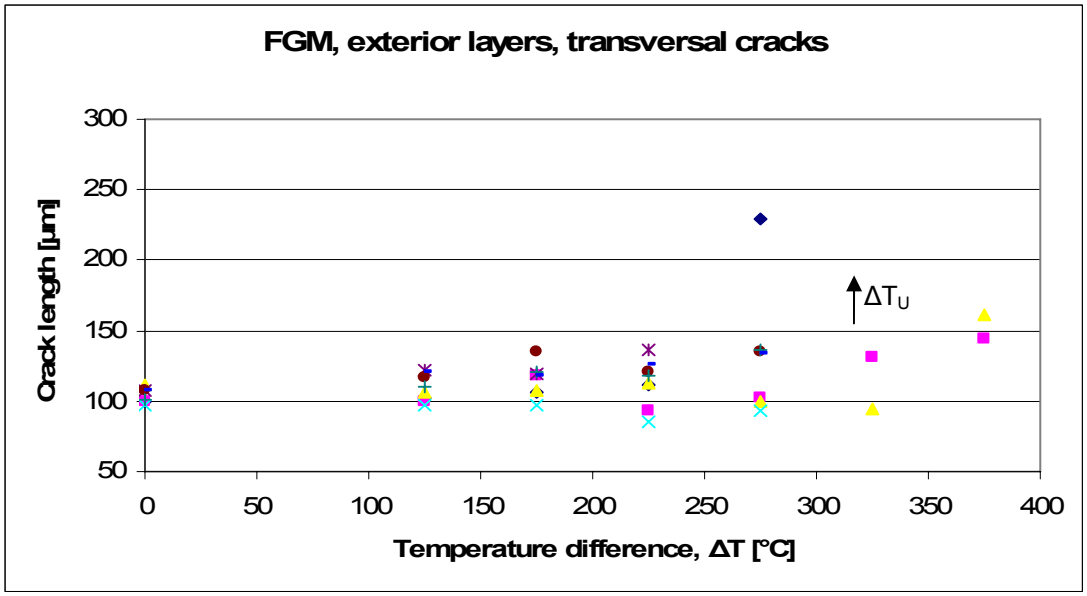

Fig. 5.13 Crack propagation of the transversal cracks in the outer layers of the graded material as a function of temperature difference. The temperature difference for unstable cracking is shown with an arrow.

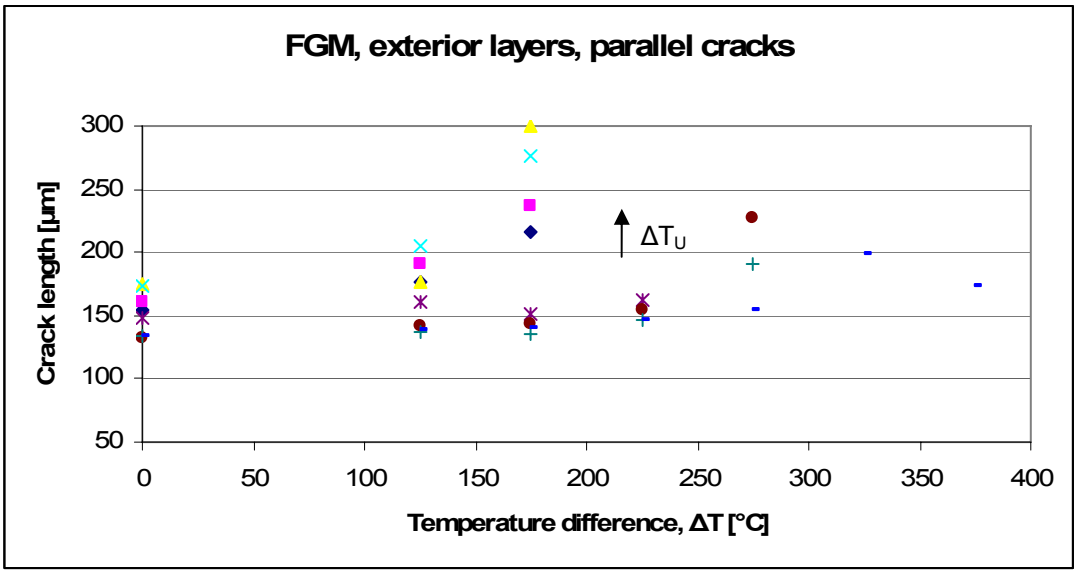

Fig. 5.14 The crack propagation of the parallel cracks in the outer layers of the graded material as a function of temperature difference. The temperature difference for unstable cracking is shown with an arrow.

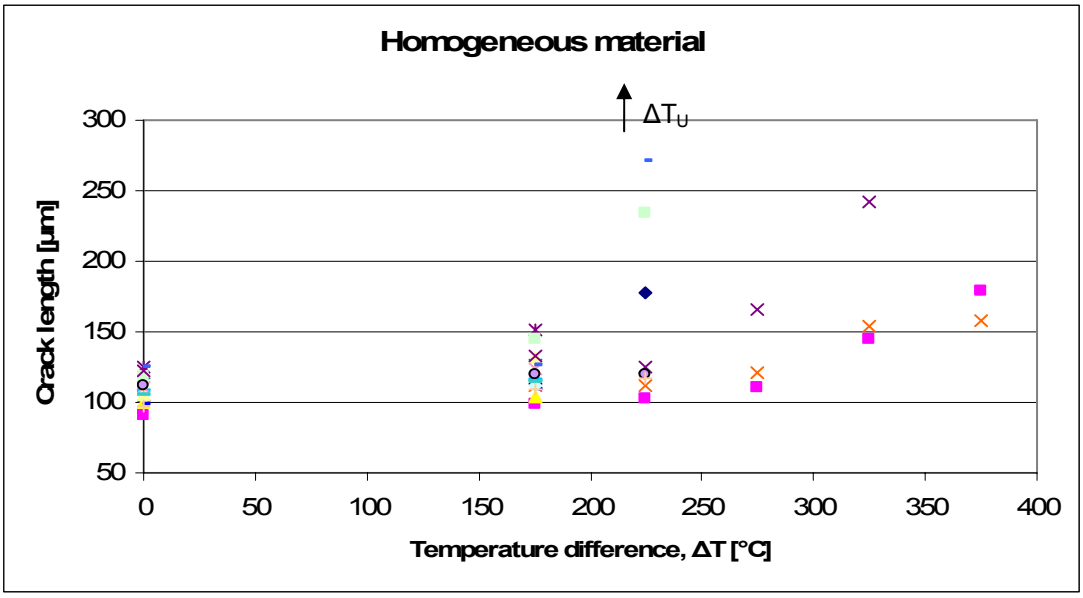

Fig. 5.15 Crack propagation in the graded material as a function of temperature difference. The temperature difference for unstable cracking is shown with an arrow.

In the interior layer the transversal cracks had grown about 20 to 30 percent already at temperature differences of 175°C, and at the temperature difference 225°C all but one crack had grown uncontrollably. At the same temperature difference the parallel cracks were rather stable, but at the temperature difference of 325°C they started to grow uncontrollably. An interesting observation is that the transversal cracks ceased to propagate when they had reached the exterior layers or the parallel cracks of the exterior layers. This is shown in figure 5.18 and can also be seen in the upper part of figure 5.16.

In the exterior layer the inverse phenomena can be seen due to the inverse stresses. The cracks began to propagate in the parallel direction already at low temperature differences whereas the transversal cracks were rather stable and did not propagate much at the same temperatures differences. It was first at 275 degrees Celsius that the transversal cracks started to propagate of considerable proportions and at 325°C five of eight cracks had grown uncontrollably. The parallel cracks had already propagated notably at a temperature difference of 125 to 175 degrees Celsius and at 225°C four of eight cracks had grown uncontrollably.

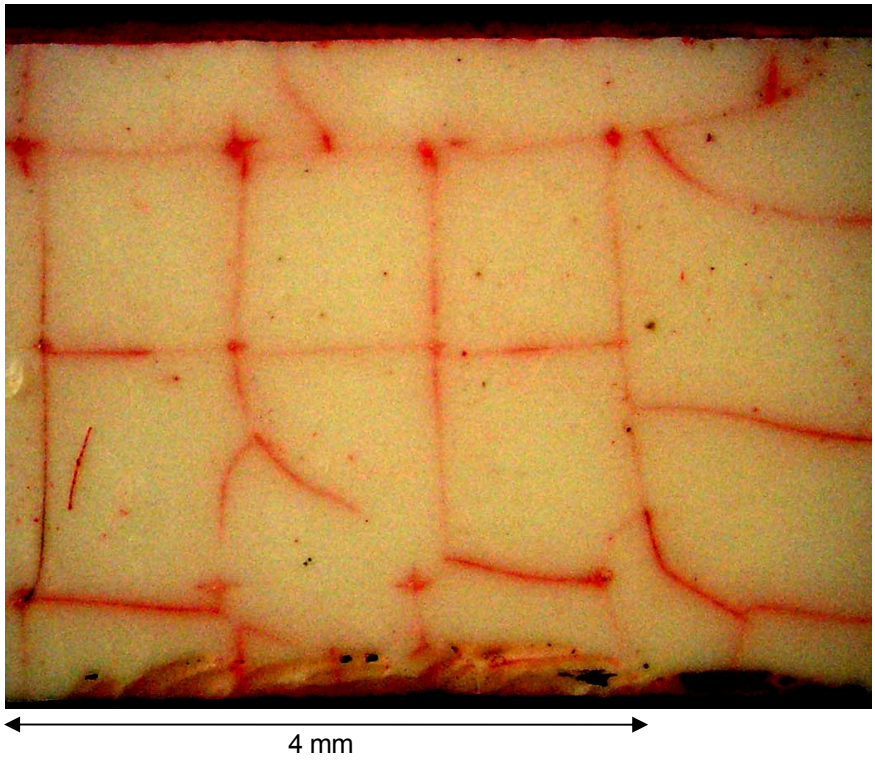

Fig. 5.16 The graded material after the thermal shock test. The indentations and the cracks are highlighted in red.

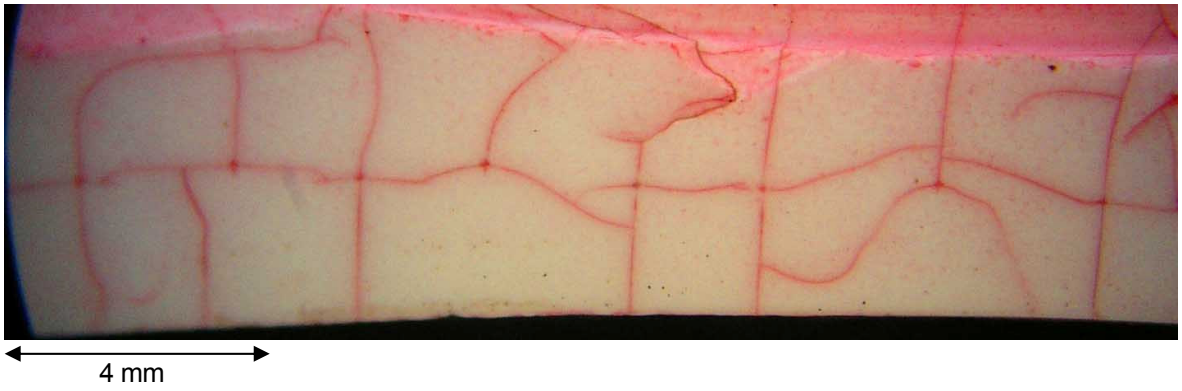

Fig. 5.17 The homogeneous material after the thermal shock test. The indentations and cracks are highlighted in red.

For the homogeneous specimen the cracks were not divided up into parallel and transversal directions since there are no differences in residual stress. Already after the first quench at the temperature difference of 175°C the cracks had grown up to 50%. After 225°C more than half of the cracks had either grown more than 100% or they had grown uncontrollably and connected themselves with other cracks. At the temperature difference of 275°C all but three cracks had grown uncontrollably. As can be seen in the figure 5.17 the cracks did not stop before the edges as they did in the graded material.

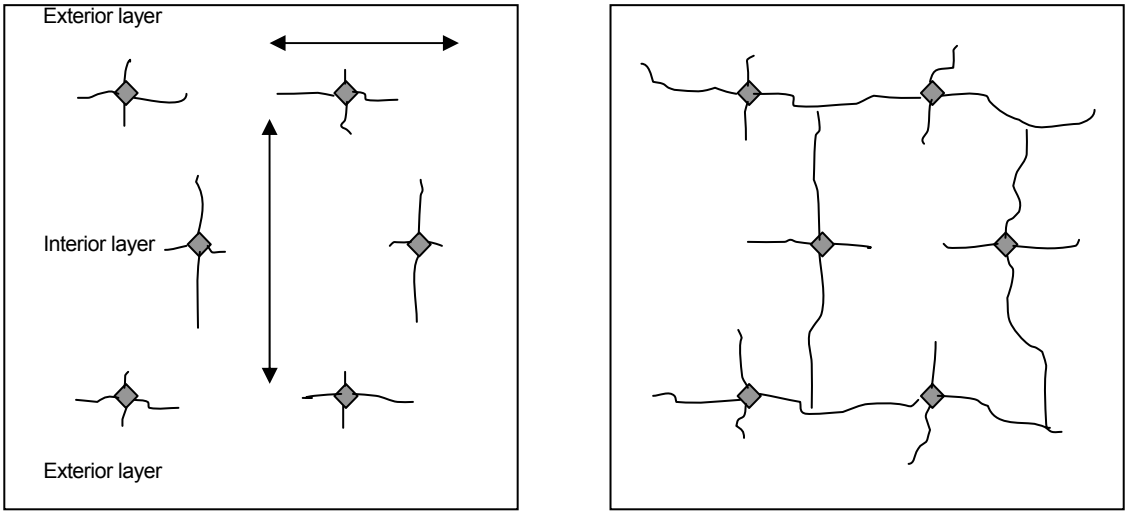

Fig. 5.18 Scheme of how the thermal shock cracking occurred in the functionally graded material. The arrows mark the principal growth directions. The left picture shows the cracking after the first thermal quenches. The right picture shows the cracking after the final thermal quenches.

The conclusion of the thermal shock test is that the graded specimen has a very good property, namely the ability to stop cracks propagating from the interior layers of the specimen before they reach the edges. This property, due to compression stresses, decreases the chances of complete breakdown of the material considerably.

Conclusions

The microstructure and mechanical properties of an Al_2O_3 - 10vol% ZrO_2 / Al_2O_3 - 30vol% ZrO_2 / Al_2O_3 -10vol% ZrO_2 functionally graded material prepared by electrophoretic deposition have been studied.

The SEM study showed that the material had a high quality fine grained microstructure with very little porosity and uniformly distributed ZrO_2. The presence of the ZrO_2 grains effectively hindered the growth of alumina matrix grains. From the SEM observation precise layer dimensions were found.

Hardness and fracture toughness, as well as the residual stresses were studied using indentation methods on the cross-section of the specimen. Their changes with respect to the compositional profile were found. The material exhibited excellent hardness in the exterior layers, comparable to that of pure alumina.

The values of the measured residual stresses were compared to those calculated by a finite element method simulation and also by a simple laminate model. The calculations tended to overestimate the maximum stresses by 10-80%. The largest differences were found in parts of the exterior layers where the compressive residual stresses should have reached maximum but were relieved probably by free surface effects.

The influence of the residual stresses on the crack propagation as a function of temperature changes was studied by means of thermal shocks using the indentation-quench method. Even at ΔT=275 °C only one of eight transversal cracks introduced into the exterior layers had grown to reach the surface, exhibiting thus highly enhanced resistance of these layers against propagation of surface cracks, which in real applications might form by impacts, wear or other contact mechanisms during the use, into the bulk. Similarly important was that no observable transversal crack originated from the side surfaces of the specimen, even though these were not polished. This can be contrasted to the crack propagation in the homogeneous material, where no preferential directions for crack growth and no crack arresting were observed.

The results show a hard surface that is subjected to compressive stresses. This together with the toughness implied by the zirconia and the generally good corrosion and creep resistance in ceramic materials leads to the conclusion that this material should work very well in structural applications where it might be in contact with other materials.

Acknowledgments

I would like to thank Dr. Pavol Hvizdoš for his guidance, enthusiasm and indefatigable helpfulness. Help and counsel with FEM analysis from Frank Dambakizi are also gratefully acknowledged

Literature

References

[1] B. KIEBACK, A. NEUBRAND, H. RIEDEL. Processing techniques for functionally graded materials. *Materials Science and Engineering* A362 (2003), pp. 81-105.

[2] D. CASELLAS [et al.]. Fracture toughness of alumina and ZTA ceramics: microstructural coarsening effects. *Journal of Materials Processing Technology* 143-144 (2003), pp. 148-152.

[3] D. J. GREEN, P. Z. CAI, G. L. MESSING. Residual stresses in Alumina-Zirconia Laminates. *Journal of the European Ceramic Society* Vol. 19 (1999) pp. 2511-2517.

[4] E. HARSANYI. U.S. Patent Number 1897902. 1933.

[5] G. C. MARQUÉS. Modelización mediante el método de los elementos finitos de tensiones residuales en recubrimientos y multicapas: aplicación en tres materiales concretos. Master's thesis. Barcelona, ETSEIB 2003.

[6] G. R. ANSTIS [et al.]. A Critical Evaluation of Indentation Techniques for Measuring Fracture Toughness: I. Direct Crack Measurements. *Journal of the American Ceramic Society* Vol. 64 (1981), pp. 533-538.

[7] J. VLEUGELS [et al.]. Thick Plate-Shaped Al_2O_3/ZrO_2 Composites with Continuous Gradient Processed by Electrophoretic Deposition. Functionally Graded Materials VII, Trans Tech Publications Ltd., Switzerland (2003) pp. 171-176.

[8] M. POPA [et al.] Residual stress profile determined by piezo-spectroscopy in alumina/alumina-zirconia layers separated by a compositionally graded intermediate layer. Fractography of Advanced Ceramics 2004, Stará Lesná, Slovakia October 2004, in press.

[9] O. SBAIZERO, E. LUCCHINI. Influence of Residual Stresses on the Mechanical Properties of a Layered Ceramic Composite. *Journal of the European Ceramic Society* 16 (1996) pp. 813-818.

[10] P. PETTERSSON, M. JOHNSSON, Z. SHEN. Parameters for measuring the thermal shock of ceramic materials with an indentation-quench method. *Journal of the European Ceramic Society* 22 (2002) pp. 1883-1889.

[11] P. SARKAR, P. S. NICHOLSON. Electrophoretic Deposition (EPD): Mechanisms, Kinetics and Application to Ceramics. *Journal of the American Ceramic Society* Vol. 79, No. 8 (1996) pp. 1987-2002.

[12] R. MORRELL. Handbook of properties of technical and engineering ceramics, Part 1, HMSO, London 1985.

[13] S. SURESH, A. MORTENSEN. Fundamentals of Functionally Graded Materials. Processing and Thermomechanical Behaviour of Graded Metals and Metal-Ceramic Composites. ASM International and The Institute of Materials, Cambridge, 1995.

[14] T. BURG, O. STANDARD. Biomedical Materials. School of Material Science and Engineering, University of New South Wales 2001.

[15] W.H. GITZEN. Alumina as a ceramic material, *The American Ceramic Society*, Columbus, Ohio 1970.

Complementary literature

[16] H. M. CHAN. Layered Ceramics. Processing and Mechanical Behaviour. *Annual Review Material Science* 27 (1997), pp. 249-82.

[17] M. COLLIN, D. ROWCLIFFE. Analysis and Prediction of Thermal Shock in Brittle Materials. *Acta Materialia* 48 (2000), pp. 1655-1665.

[18] P. HVIZDOŠ [et al.]. Mechanical Properties of Alumina/Zirconia Functionally Graded Material Prepared by Electrophoretic Deposition. Fractography of Advanced Ceramics 2004, Stará Lesná, Slovakia, October 2004, in press.

[19] P. Z. CAI, D. J. GREEN, G. L. MESSING. Mechanical Characterization of Al_2O_3/ZrO_2 Hybrid Laminates. *Journal of the European Ceramic Society* 5 (1998) pp. 2025-2034.

[20] W. D. CALLISTER, JR. Materials Science and Engineering, An Introduction. John Wiley & Sons, Inc. New York 1994